AMPK blocks chromatin activation and consequent R-loop formation to protect genome stability following acute starvation

Bing Sun
Umass Medical School https://orcid.org/0000-0002-1992-3767
McLean Sherrin
McGill University
Richard Roy (richard.roy@mcgill.ca)
McGill University

Article

Keywords: C. elegans, R-loop, transcriptional elongation, H3K4me3, DNA damage, RAD-51, germ line, transgenerational epigenetic inheritance

Posted Date: April 9th, 2021

DOI: https://doi.org/10.21203/rs.3.rs-378687/v1

Abstract

During periods of starvation organisms must modify both gene expression and metabolic pathways to adjust to the energy stress. We previously reported that *C. elegans* that lack AMPK have transgenerational reproductive defects that result from abnormally elevated H3K4me3 levels in the germ line following recovery from acute starvation[1]. Here we show that H3K4me3 is dramatically increased at promoters, driving aberrant transcription elongation that results in the accumulation of R-loops in the starved AMPK mutants. DRIP-seq analysis demonstrated that a significant proportion of the genome was affected by R-loop formation with a dramatic expansion in the number of R-loops at numerous loci, most pronounced at the promoter-TSS regions of genes in the starved AMPK mutants. The R-loops are transmissible into subsequent generations, likely contributing to the transgenerational reproductive defects typical of these mutants following starvation. Strikingly, AMPK null germ lines show considerably more RAD-51 foci at sites of R-loop formation, potentially sequestering it from its critical role at meiotic breaks and/or at sites of induced DNA damage. Our study reveals a previously unforeseen role of AMPK in maintaining genome stability following starvation, where in its absence R-loops accumulate, resulting in reproductive compromise and DNA damage hypersensitivity.

Introduction

In most organisms a highly conserved enzyme called AMP-activated protein kinase (AMPK) acts as a metabolic master regulator through its ability to sense reduced energy levels[2]. In situations of stress it phosphorylates target proteins to ensure that energy is appropriately allocated within an organism[1–3]. We noted previously that *C. elegans* that lack this important metabolic sensor are often sickly, have reduced brood sizes, or are sterile following their recovery from acute starvation[1]. What is more intriguing is that these reproductive phenotypes are transmitted to subsequent generations of animals that were never starved, suggesting that a molecular memory of the stress is transmitted to future generations when this enzyme is disrupted. Later generations show spontaneous somatic mutant phenotypes, much like mutant animals that lack histone demethylase activity[4,5], and often become sterile after one to several (up to 10) generations.

The transgenerational reproductive defects can also occur at very low frequency in wild type (WT) animals that are starved for extended durations[6]. This suggests that the epigenetically inherited reproductive defects documented in the descendants of mutants that lack AMPK signalling very likely reflect the extreme effects of starvation on the germ line, although they occur after a much shorter delay in these mutants. This transgenerational epigenetic inheritance has been observed in several contexts in *C. elegans* and the progressive mortalization of the germ line is often associated with aberrant changes in the histone modifications typically present in the affected germ cells[7–9].

Results

The primordial germ cells (PGCs) of starved AMPK mutant L1 larvae have abnormally high levels of nuclear localized SET-2, an MLL/SET1-like H3K4 histone methyltransferase that is likely responsible for the observed increase in trimethylated histone H3 at lysine 4 (H3K4me3), resulting in the inappropriate activation of transcriptional elongation in some genes[1,10]. Since the F_2 generation is the first generation that was not directly exposed to the starvation[11], we performed ChIP-seq to generate genome-wide H3K4me3 maps from the F_2 adult descendants of starved AMPK mutant L1 larvae[12] (the first transgenerational brood) (Fig. 1a). Consistent with our previous findings, H3K4me3 levels are abnormally high in the F_2 descendants of starved AMPK mutants, while additional "ectopic" sites of deposition that diverge from the wild-type pattern of R-loop-associated loci, result in a strikingly distinct H3K4me3 signature in the *aak-1/2* mutant animals compared to WT adult hermaphrodites, with 31 additional ectopic sites (Supplementary Fig. 1a).

H3K4me3 is found primarily on chromatin near or around proximal promoters or transcription start sites (TSSs)[13]. Consistent with this feature, we noted a high proportion of the "ectopic" H3K4me3 peaks identified in the descendants of starved AMPK mutants at, or around, promoter regions (Fig. 1b and Supplementary Fig. 1b). Annotation and peak location statistics reveal that the F_2 descendants of starved AMPK mutant hermaphrodites (*aak-1/-2*) harbour more H3K4me3 signals spanning TSSs when compared to WT adults (Fig. 1c,d and Supplementary Fig. 1c-e). Further global analysis of H3K4me3 signals indicated that ~ 88% of the peak calls in *aak-1/2* mutants accumulate at promoter-TSSs, while only ~ 36% are found at such loci in WT animals (Fig. 1e).

Blocking the formation of H3K4me3 at TSS-proximal regions is critical for early embryonic development in *C. elegans*[14]. We identified that 40% of the total H3K4me3 was deposited at proximal regions (2 kb upstream of TSS) in *aak-1/2* mutants compared to only ~ 24% in WT animals (Supplementary Fig. 2), suggesting that the “ectopic” deposition of these H3K4me3 marks could generate an abnormal transcription-activating signal at the TSS-proximal regions of these genes.

Transgenerational H3K4me3 accumulation at TSSs may thus result in robust, but inappropriate, gene expression in starved AMPK mutants. If the synthesis of these gene products becomes miscoordinated with post embryonic developmental progression, their aberrant expression could negatively impact cellular homeostasis and/or growth. To determine if this aberrant transcription contributes to the starvation-induced sterility that occurs in the absence of AMPK signalling through untimely protein synthesis, we treated the starved mutants with the translation inhibitor cycloheximide (CHX) during the diapause and evaluated sterility following recovery in replete growth conditions. Unlike the treatment with the specific transcription elongation inhibitor, 5,6-dichloro-1-β-D-ribofuranosylbenzimidazole (DRB)[1], blocking translation had no differential effect on the starvation-induced sterility of these AMPK mutants (Fig. 2a, b). These results strongly suggest that the starvation-induced reproductive defects typical of AMPK mutants arise from the inappropriate transcription/elongation that occurs in the PGCs, or potentially from the RNA products that are generated by these animals during starvation.

Efficient transcriptional elongation only occurs following multiple changes within the post-initiation RNA Polymerase II complex that enhance RNA processing and processivity[15,16]. In the absence of these components the elongating complex can pause until these contingencies are satisfied[17,18]. In some cases the nascent preRNA that is associated with these stalled complexes can thread back into the transcription bubble, where it can base pair with the non-coding strand of DNA. These triplexes are referred to as R-loops, and they are abundant non-B DNA structures formed by co-transcriptional DNA-RNA hybrids that can occur during transcriptional pausing[19] (Fig. 4g). Their presence in the genome is strongly selected against due to their propensity to cause mutations. R-loop occurrence is associated with replication/transcription conflicts that result in DNA damage, while they are also a source of genome instability resulting from single nucleotide changes catalyzed by DNA modifying enzymes such as cytidine deaminases that can access the vulnerable single stranded DNA corresponding to the coding strand of expressed genes[20].

Because these structures can cause genome instability that could be transmitted throughout successive generations, we probed the germline DNA from the F_2 descendants of starved AMPK mutants for the presence of R-loops. In parallel, we stained the germ line of a mutant that is deficient for the Tho-Trex complex (*thoc-2*) that results in an increased abundance of R-loops[21]. Our analysis indicated that the AMPK mutant (*aak-1/2*) germ lines displayed significantly higher levels of R-loop foci compared to WT (Fig. 2c), which could be partially alleviated by microinjecting RNaseH enzyme[22] or *rnh-1*-expressing transgenes into the gonad (Supplementary Fig. 3a,c), or by inhibition of inappropriate transcriptional elongation with DRB during periods of starvation (Supplementary Fig. 3b). Like the H3K4me3 levels[1], the abnormal abundance of R-loops was gradually resolved over multiple generations, whereby R-loop numbers were most abundant in the germ cells of animals following starvation in P_0 adults > F_2 descendants > F_5 descendants (Fig. 2b).

To better understand if a specific class of genes were prone to R-loop formation in the absence of AMPK during starvation, high-throughput sequencing and analysis of genomic DNA-RNA hybrids by immunoprecipitation (DRIP-seq) was performed identically to the H3K4me3 ChIP-seq experiments, using genomic DNA obtained from the F_2 generation of starved WT and *aak-1/2* animals (Supplementary Fig. 4a). We noted a dramatic expansion in the number of R-loops at loci that had not previously been associated with these structures, but also in the overall abundance throughout the entire genome (Supplementary Fig. 4b) in the F_2 descendants of starved *aak-1/2* mutants compared to WT F_2 controls by comparing both read coverage and depth (Fig. 2e, f), with high reproducibility between biological replicates (Supplementary Fig. 5a, b). The specificity of the S9.6 antibody that recognizes the DNA-RNA hybrids was corroborated by the decrease in germline signal detected upon RNaseH treatment, consistent with these RNaseH-sensitive loci being R-loops (Fig. 2e).

The locus-specific enrichment of R-loops was validated by DRIP-qPCR in which some (~ 50%, Supplementary Fig. 3b) of the enhanced R-loops in the F_2 descendants of starved *aak-1/2* mutants could

be resolved by blocking elongation during the period of starvation, while others remained unchanged (*cit-1.2*; Fig. 2g).

Genome wide DRIP-seq allowed us to identify a significant proportion of the genome (3.1% and 4.7% in the F_2 descendants of starved WT and AMPK mutants, respectively) involved in R-loop formation in *C. elegans* (Supplementary Fig. 5d). In both WT and *aak-1/2* mutants, a high number of genomic regions that were associated with R-loops were conserved between the two genotypes (Supplementary Fig. 5c), suggesting the presence of a common R-loop forming feature in, or around these loci[23]. As has been reported in *Saccharomyces cerevisiae*[24]and human cells[25], R-loops are not restricted to nuclear genes, since we also detect them in the mitochondrial genome of *C. elegans* (Supplementary Fig. 4b, c). In *Drosophila*, R-loops are highly enriched in repetitive DNA sequences such as satellite DNAs[26]. We also observed that a substantial number of R-loops arise within satellite DNA regions, preferentially at centromeric heterochromatin, in the F_2 descendants of starved AMPK mutants (Supplementary Fig. 5e).

GC skew also contributes to R-loop formation in humans[19,26]. The genomic sequence present within the extracted R-loop peaks from 1 kb up- and downstream exhibit strong GC skew in *C. elegans*, especially in the regions adjacent to the R-loop peaks (Fig. 3a). Although AT skew[27] was not revealed in our genome-wide analysis, we did note that there are a substantial number of R-loop-associated sequences with strong AT skew in *C. elegans* (Supplementary Fig. 6), especially in the F_2 descendants of starved AMPK mutants (Fig. 3b). Two polypyrimidine sequences and two poly(A) tracts were identified by HOMER *de novo* motif analysis (Fig. 3b) in AMPK mutant *versus* WT DRIP-seq, suggesting the possibility that a subset of R-loops can form in sequences associated with trans-splicing and polyadenylation[23,24], but only in the F_2 descendants of previously starved animals that lack all AMPK signalling[28,29].

Our genome-wide analyses indicate that overall R-loop intensity in *C. elegans* is most pronounced at the promoter-TSS region (Fig. 3c and Supplementary Fig. 7a-c). Notably, R-loops accumulating at the promoter-TSS region occupy ~ 2.4% of the genome in the F_2 descendants of previously starved AMPK mutant animals, compared to only ~ 1.7% in WT. Besides the promoter-TSS regions, R-loops at transcription termination sites (TTSs) occupied nearly ~ 20% of the total peaks (Fig. 3c), which is comparable to estimates of prevalent and conserved R-loop formation at promoter and terminator regions of Pol II-dependent genes in human and mouse genomes[30,31]. Among those genes with common promoter-associated R-loops in WT and the F_2 descendants of starved AMPK mutant animals, only ~ 5.6% share R-loops at the corresponding TTS regions (Supplementary Fig. 7d), suggesting that distinct mechanisms are involved in the regulation of R-loop dynamics at these two intragenic hotspots.

In contrast, the proportion of R-loop peaks in the intron and intergenic regions was relatively low in both samples (Fig. 3c and Supplementary Fig. 7a, b). Notably, genome-wide R-loop signal distribution was increased over intergenic regions following AMPK depletion (Fig. 3d), suggesting potential functions of AMPK in regulating R-loop formation potentially by restricting the expression of intergenic sequences[32]. Considering that our H3K4me3 ChIP-seq and DRIP-seq signals have similar distribution patterns at the

promoter-TSS regions in the F_2 descendants of starved AMPK mutant animals (Fig. 1e and Fig. 3c), and that genes with promoter-localized R-loops coincide with significantly higher transcription activity of the resident genes[30], our data suggest that the increased abundance of conserved and ectopic H3K4me3 deposition that we observe in the F_2 descendants of starved AMPK mutant animals positively correlates with the formation and/or maintenance of R-loops (Fig. 3e, f).

Persistent, unresolved R-loops can promote DNA damage and genomic instability[26,33]. Elevated R-loop levels strongly correlate with sites of replication-stress-induced DNA damage[34]. We noted that the F_2 descendants of starved AMPK mutant animals were hypersensitive to hydroxyurea (HU) and the alkylating agent methyl methanesulfonate (MMS), both of which are genotoxic drugs that compromise DNA replication[35] (Fig. 4a,b and Supplementary Fig. 8a). These findings suggest that starved AMPK mutant descendants are hypersensitive to DNA damage and/or replication stress, potentially due to the increased abundance of R-loops.

The RecA ortholgue RAD-51 recombinase plays a critical role in the recognition of damage sites and their eventual repair[36,37]. During meiosis, the DSBs typical of meiotic intermediates are also recognized and bound by RAD-51 in the *C. elegans* germ cells[38,39]. We observed considerably more RAD-51 foci (markers of DSB repair intermediates) in each zone of the adult germ line in the descendants of starved AMPK mutants compared with WT (Fig. 4b,c). Moreover, we noticed that nuclei with highly abundant RAD-51 foci often appeared in the AMPK mutant germ lines (Fig. 4c), suggesting that these nuclei may have irreparable damage and are destined for elimination. Indeed, we observed an increased abundance of CED-1::GFP positive cells indicating that the frequency of apoptotic cell death[21] was significantly enhanced in the germ lines of the descendants of starved AMPK mutants (Fig. 4d and Supplementary Fig. 8b).

If the additional RAD-51 foci are due to R-loop-induced DNA damage, at least some of these additional RAD-51 foci may localize to R-loop containing loci. We therefore determined the physical overlap between RNA-DNA hybrids and RAD-51 in the germ lines of the descendants of starved AMPK mutants using a proximity ligation assay (PLA) that detects interactions to a limit 30 ~ 40 nm[40]. Our results indicate that RAD-51 is localized to R-loops at some of these supernumerary RAD-51 foci, while positive PLA signals were undetectable in WT germ lines (Fig. 4e and Supplementary Fig. 8c). These results suggest that DNA damage is likely induced at these R-loops, potentially due to transcription-replication conflicts that arise in the mitotic zone and persist, or alternatively, it may represent collateral sites of damage that arise during the process of R-loop resolution[41]. If RAD-51 is sequestered at these sites it could potentially limit is normal involvement in meiotic break resolution, potentially contributing to the sterility observed in the AMPK mutant adults that were previously starved as emergent larvae. To determine if RAD-51 might be limiting in the germ line due to its sequestration at R-loops, we drove the expression of an extrachromosomal array of RAD-51 in the germ cells of AMPK mutants. Providing additional copies of RAD-51 partially suppressed the sterility of AMPK mutant hermaphrodites that were subjected to acute starvation during the L1 stage (Supplementary Fig. 8d). Taken together, these data suggest that *C.*

elegans larvae that lack all AMPK signalling ectopically deposit H3K4me3 marks that trigger aberrant transcriptional elongation resulting in an increased frequency of R-loop formation during periods of energy stress. These sites are transmissible along with their H3K4me3 marks, and are prone to DNA damage leading to RAD-51 sequestration, thus resulting in abnormal reproductive development, enhanced germline apoptosis, and ultimately culminating in sterility (Fig. 4g).

Discussion

The importance of developmental quiescence is most clearly revealed in the phenotypes associated with its untimely reversal[1,42–46]. The misregulated gene expression associated with aberrant SET1/MLL-mediated chromatin activation is well known to result in various forms of tumours and/or inappropriate developmental outcomes[47]. Using *C. elegans* as a model, we show that the protein kinase AMPK links physiological and/or metabolic status to adaptive changes in gene regulation. In the case of early larval development, its compromise is detrimental, causing premature expiration or subsequent sterility that can arise over several generations[1].

Although the reason for the lethality of AMPK mutants subjected to acute starvation remains unclear, it is likely associated with inappropriate energy allocation to vital functions. On the other hand, the sterility can be improved by simply blocking inappropriate transcriptional elongation, but not by eliminating untimely protein synthesis.

Our findings suggest that an increase in the H3K4me3 marks that accumulate in starved AMPK mutants results in a consequent increase in R-loop formation, presumably due to prematurely activated RNA Polymerase II complexes that stall proximally to the TSS. The nascent pre-mRNA may then thread back to form R-loops at these sites, that are either not resolved immediately and persist into the adult germ line, or are consistently reformed during germ line development, generating sites of DSB that are bound by RAD-51.

The titration of RAD-51 may be highly relevant both immediately following the L1 diapause and/or later during meiosis. The early stages of post-embryonic development are associated with a rapid increase in gene expression that, like in other organisms, is associated with a concomitant increase in DNA damage that include DSBs and RAD-51 intervention[48–50]. Similarly, during meiosis, RAD-51 is required to bind to recombination intermediates to stabilize and protect these structures during strand invasion and resection. If RAD-51 is stably bound to R-loops it may be limiting for its function in resolving the DSBs that arise in both cases, resulting in soma/germ line developmental asynchrony in one case, and meiotic failure in the other. Both of which are consistent with the gonadal phenotypes we observe in the starved AMPK mutant adults.

Although the increased frequency of R-loops in the starved AMPK mutants is resolved in 5 generations, the consequences of these mutagenic structures may persist for much longer. During the period that the triplex remains unresolved, the coding strand is highly vulnerable to sequence-altering enzymes. These

modifications are among the most common mutations detected in a wide array of cancer types[51], suggesting that these enzymes are both prevalent and highly active. The undetected nucleotide substitution can become fixed, giving rise to a permanent genetic change that persists long after the R-loop has been resolved. This may also account for some of the observed spontaneous phenotypes that arise in later generation AMPK mutants that were previously starved, or in the late generation *spr-5* mutants, which also have a genome-wide increase in H3K4me2, another transcription-activating chromatin mark that arises due to the lack an LSD1-like histone demethylase[5].

The genome instability and compromised germ line integrity that arises in these starved AMPK mutants due to the increased R-loop frequency is almost certainly not adaptive. On the other hand, it does generate a previously unexpected source of genetic diversity that arises during an otherwise desperate, yet evolutionarily relevant challenge, that being starvation. The maladaptive consequences of these starvation-induced epigenetic modifications may nevertheless presage genetic change or even enhance genetic diversity in these compromised animals. These seemingly maladaptive responses to starvation described here are not without parallels in other contexts of environmental challenge. Microbes have adopted several surprising mechanisms of increasing genetic diversity during environmental challenges, ranging from relaxing interspecies barriers to mating[52], to full random resectionning/recombination of their chromosomes following irradiation[53]. The R-loops that form in this context may represent a similar double-edged sword by providing animals with an increased rate of genetic change accompanied by a corresponding fitness trade off.

Methods

C.elegans Strains and Genetics

C. elegans were cultured at 20°C on OP50. Strains used in this study include: Bristol N2 wild type, *aak-1(tm1944)* III; *aak-2(ok524)* X, *thoc-2(tm1310)* III/ *hT2[bli-4(e937) let-?(q782) qIs48]* (I;III) and *smIs34*.

Reagents and Antibodies

Methyl methanesulfonate (129925, Sigma-Aldrich), hydroxyurea (H8627, Sigma-Aldrich), Agencourt AMPure XP (A63880, Beckman Coulter), 4,6-Diamidino-2-phenylindole (DAPI, 10236276001, Roche), Halt Protease and Phosphatase Inhibitor Cocktail (1861281, Thermo Scientific), VECTASHIELD Antifade Mounting Medium (H-1000, Vectorlabs), RNase H (M0297, NEB) and cycloheximide (1041-1, BioVision). The following antibodies were used: anti-DNA-RNA hybrid, clone S9.6 (MABE1095, Millipore), anti-RAD-51 (gift from Monique Zetka), anti-H3K4me3 (ab8580, abcam), Goat anti-Rabbit IgG (H + L) Highly Cross-Adsorbed Secondary Antibody, Alexa Fluor 488 (A-11034, Invitrogen) and Goat anti-Mouse IgG (H + L) Highly Cross-Adsorbed Secondary Antibody, Alexa Fluor 594 (A-11032, Invitrogen).

ChIP-Seq and DRIP-seq

L1 hatchlings were maintained 3 days in sterile M9 buffer without bacteria[1]. After this period L1 larva were transferred to NGM plates and fed for two generations until F2 adults were harvested to generate extracts for both ChIP and DRIP. Immunoprecipitation was performed from 3 biological repeats. DRIP in *C. elegans* was performed as described with minor modifications[54]. Primers used for DRIP-qPCR are as follows: *tig-3* (forward: 5'-ACTCCAAATGCTCTAAGTACAACTG-3', reverse: 5'-ACACAGTGTGCTCCACAG-3'); *K07C5.6* (forward: 5'-CCTTCTCGCGTTCTTTTTCTTTTTC-3', reverse: 5'-CAAAGTTCCGAAGTTAGTAGAGAAGAC-3'); *cit-1.2* (forward: 5'-GCTCTTTATTTGGGTTCAATTCCTG-3', reverse: 5'-GTCGACAACAAGAGTGGAAACC-3') and *rrn-3.56* (forward: 5'-CCCACAGATCTACTATATTAAATGTGCCC-3', reverse: 5'- TCCCCGCTTGACACTGT-3').

The libraries were prepared and sequenced by Institute for Research in Immunology and Cancer (IRIC) in Montreal. The sequencing data were obtained using an Illumina Nextseq instrument and data were analyzed with the ChIP-seq pipeline implemented by the Canadian Center for Computational Genomics. Reads were trimmed from the 3' end to have a phred score of at least 30[55]. Illumina sequencing adapters were removed from the reads, and all reads were required to have a length of at least 50 bp. Trimming and clipping were performed using Trimmomatic[55]. The filtered reads were aligned to ce11 genome (*Caenorhabditis_elegans* assembly WBcel235). Each readset was aligned using Burrows-Wheeler Aligner (BWA) algorithm[56] which creates a Binary Alignment Map file (.bam). Then, all readset BAM files from the same sample were merged into a single global BAM file using Picard. Base quality filtering of the aligned reads was then performed based on the quality of the BAM file, where each alignment file per sample was filtered using SAMtools[57]. All alignments with MAPQ smaller than 20 and samflag 4 (read unmapped) are excluded from the resulting file in BAM format. Duplicated aligned reads that have the same 5' alignment positions were made with Picard. All but the best pair (based on alignment score) was marked as a duplicate in the BAM file. Duplicate reads were excluded from subsequent analysis.

To facilitate the analysis of ChIP-Seq, the HOMER software[58] was used to transform the sequence alignment into a platform independent data structure representing the experiments. All relevant information about the experiment was organized into a 'Tag Directory'. During the creation of tag directories, several quality control routines were run to help provide information and feedback about the quality of the experiment. BedGraph track format files were generated from the aligned reads using HOMER. Peaks were called using MACS software[59] and were annotated with HOMER using RefSeq annotations. Gene ontology and genome ontology analyses are also performed at this stage by DAVID functional annotation bioinformatics microarray analysis https://david.ncifcrf.gov[60]. De novo motif analyses were also performed with HOMER.

Visualization of superimposed track heat maps

EaSeq software[61] was used for visualization to generate superimposed track heat maps as previously described[13]. The .bam files were imported using default settings and all values were normalized to reads per kilobase million (RPKM). Line tracks of the superimposed signal were generated using the ‘LineTrack’ tool, 1000 bp surrounding each region was segmented into 400 bins and smoothed for 1 bin. Heat maps

were made by the 'HeatMap' tool. The 'Colocalize' tool was used to determine the distances from and orientation of each TSS to the nearest peak centre. Heat maps were ordered according to increasing size using the 'Sort' tool.

RAD-51 and RNH-1 overexpression lines

Genomic *rad-51* and *rnh-1.0* were amplified and cloned into pBluescript vector by Gibson assembly. Primers used for PCR are: *rad-51* (forward: 5'-ATGGGACAATCTTGGGGATATGAAG-3', reverse: 5'-CTAGTCCTCGCGTGCGTCCT-3') and *rnh-1* (forward: 5'-ATGAGCAAGTTCTATGGTGTGG-3', 5'-TCAAAATCTGAAATTTTTCAAGTTTTGAGT-3'. The *pie-1* promoter and the *pie-1* 3' UTR were used to drive germline expression throughout development. Transgenic lines were generated by microinjecting constructs at 1ng/ul as a complex array with rol-6 marker.

Drug treatments

CHX treatment of L1 larvae during starvation was performed as described previously with DRB[1]. Briefly, wild-type and *aak-1/2* L1 larvae obtained by alkaline hypochlorite treatment were maintained in M9 buffer without or with 20 µM CHX during the 3 day period of diapause. Following this period, L1 larvae were transferred to OP50-seeded NGM plates and when they reached the L4 stage 50 larvae per condition were isolated and after 3 days their fertility and brood size were assessed. Experiments were performed at least thrice. HU and MMS treatments were performed according to previous descriptions[62]. For HU treatment, the synchronized L1 larvae without or with 3-day starvation in M9 buffer was transferred to OP50-seeded NGM plates containing HU of indicated concentration and treated for 48 hours before singled into plate for scoring the fertility. MMS treatment was done similarly to HU treatment except that MMS was added to the M9 buffer at the indicated concentration and treated for the last 12 hours of the 3-day starvation.

S9.6 and RAD-51 immunofluorescence

S9.6 immunofluorescence was performed as previously described[63] using secondary antibodies conjugated with Alexa 594. Immunofluorescence analysis of RAD-51 was performed as previously described[64] using secondary antibodies conjugated with Alexa 488. Immunofluorescence images were acquired and processed using a Leica DMI 6000B inverted microscope equipped with a Quorum WaveFX spinning Disc and EMCCD camera. S9.6 signal intensity and quantification of RAD-51 foci were analyzed and processed with ImageJ software. For RAD-51 foci quantification, the gonads were separated into 6 equal zones by equally dividing the number of cell rows from the distal end of the gonad to the onset of diakinesis. More than 100 cells were scored in each experiment.

Live Imaging

Animals were placed on a slide with a 3% agarose pad and a drop of 0.2 mM levamisole in M9 buffer. A coverslip was placed onto the drop and sealed with nail polish. Images were taken using spinning-disk confocal microscopy as described above.

Proximity Ligation Assay (PLA)

PLA was performed with Duolink In Situ PLA® Probe Anti-Rabbit PLUS (DUO92002, Sigma-Aldrich), Duolink In Situ PLA® Probe Anti-Mouse MINUS (DUO92004, Sigma-Aldrich) and Duolink In Situ Detection Reagents Red (DUO92008, Sigma-Aldrich) according to manufacturer's instructions. The dissected gonads were freeze-cracked with liquid nitrogen before fixation with cold methanol for 10 min. Anti-DNA-RNA hybrid (mouse, 1:50) and anti-RAD-51 (rabbit, 1:1000) antibodies were used.

Statistical analysis

All statistical analyses were performed using GraphPad Prism Software. Error bars indicate standard errors of the mean (S.E.M.) or confidence interval at 95% (95% CI) as indicated. Statistical significance was assessed by Fisher's exact test, Mann-Whitney U-test, two-tailed unpaired t-test with Welch's correction or one-way ANOVA, as indicated. Statistical significance was considered at $p < 0.05$.

Declarations

ACKNOWLEDGMENTS

We are grateful to members of the Roy and Zetka laboratories for reagents, discussion and advice. Some of the *C. elegans* strains used in this work were provided by the *Caenorhabditis* Genetics Center (Univ. of Minnesota), which is funded by the NIH National Center for Research Resources (NCRR). This study was supported by funding from the Canadian Institutes for Health Research (CIHR).

AUTHOR CONTRIBUTIONS

B.S. and R.R. planned the study, designed the experiments and wrote the manuscript with input from all coauthors. B.S. and M.S. performed the experiments. B.S. analyzed the data. R.R. supervised the work.

References

1. Demoinet, E., Li, S. & Roy, R. AMPK blocks starvation-inducible transgenerational defects in Caenorhabditis elegans. *Proc Natl Acad Sci U S A* **114**, E2689-E2698 (2017).
2. Hardie, D.G., Ross, F.A. & Hawley, S.A. AMPK: a nutrient and energy sensor that maintains energy homeostasis. *Nat Rev Mol Cell Biol* **13**, 251–62 (2012).
3. Lee, H. *et al.* Energy-stress-mediated AMPK activation inhibits ferroptosis. *Nat Cell Biol* **22**, 225–234 (2020).
4. Greer, E.L., Becker, B., Latza, C., Antebi, A. & Shi, Y. Mutation of C. elegans demethylase spr-5 extends transgenerational longevity. *Cell Res* **26**, 229–38 (2016).
5. Katz, D.J., Edwards, T.M., Reinke, V. & Kelly, W.G. A C. elegans LSD1 demethylase contributes to germline immortality by reprogramming epigenetic memory. *Cell* **137**, 308–20 (2009).
6. Jobson, M.A. *et al.* Transgenerational Effects of Early Life Starvation on Growth, Reproduction, and Stress Resistance in Caenorhabditis elegans. *Genetics* **201**, 201–12 (2015).

7. Harvey, Z.H., Chakravarty, A.K., Futia, R.A. & Jarosz, D.F. A Prion Epigenetic Switch Establishes an Active Chromatin State. *Cell* **180**, 928–940 e14 (2020).
8. Borg, M. *et al.* Targeted reprogramming of H3K27me3 resets epigenetic memory in plant paternal chromatin. *Nat Cell Biol* **22**, 621–629 (2020).
9. Barucci, G. *et al.* Small-RNA-mediated transgenerational silencing of histone genes impairs fertility in piRNA mutants. *Nat Cell Biol* **22**, 235–245 (2020).
10. Fanucchi, S. *et al.* Immune genes are primed for robust transcription by proximal long noncoding RNAs located in nuclear compartments. *Nat Genet* **51**, 138–150 (2019).
11. Skinner, M.K. What is an epigenetic transgenerational phenotype? F3 or F2. *Reprod Toxicol* **25**, 2–6 (2008).
12. Camacho, J. *et al.* The Memory of Environmental Chemical Exposure in C. elegans Is Dependent on the Jumonji Demethylases jmjd-2 and jmjd-3/utx-1. *Cell Rep* **23**, 2392–2404 (2018).
13. Dahl, J.A. *et al.* Broad histone H3K4me3 domains in mouse oocytes modulate maternal-to-zygotic transition. *Nature* **537**, 548–552 (2016).
14. Kaser-Pebernard, S., Pfefferli, C., Aschinger, C. & Wicky, C. Fine-tuning of chromatin composition and Polycomb recruitment by two Mi2 homologues during C. elegans early embryonic development. *Epigenetics Chromatin* **9**, 39 (2016).
15. Bartman, C.R. *et al.* Transcriptional Burst Initiation and Polymerase Pause Release Are Key Control Points of Transcriptional Regulation. *Mol Cell* **73**, 519–532 e4 (2019).
16. Sheridan, R.M., Fong, N., D'Alessandro, A. & Bentley, D.L. Widespread Backtracking by RNA Pol II Is a Major Effector of Gene Activation, 5' Pause Release, Termination, and Transcription Elongation Rate. *Mol Cell* **73**, 107–118 e4 (2019).
17. Shao, W. & Zeitlinger, J. Paused RNA polymerase II inhibits new transcriptional initiation. *Nat Genet* **49**, 1045–1051 (2017).
18. Skourti-Stathaki, K. *et al.* R-Loops Enhance Polycomb Repression at a Subset of Developmental Regulator Genes. *Mol Cell* **73**, 930–945 e4 (2019).
19. Manzo, S.G. *et al.* DNA Topoisomerase I differentially modulates R-loops across the human genome. *Genome Biol* **19**, 100 (2018).
20. Buisson, R. *et al.* Passenger hotspot mutations in cancer driven by APOBEC3A and mesoscale genomic features. *Science* **364**(2019).
21. Zeller, P. *et al.* Histone H3K9 methylation is dispensable for Caenorhabditis elegans development but suppresses RNA:DNA hybrid-associated repeat instability. *Nat Genet* **48**, 1385–1395 (2016).
22. Castellano-Pozo, M., Garcia-Muse, T. & Aguilera, A. R-loops cause replication impairment and genome instability during meiosis. *EMBO Rep* **13**, 923–9 (2012).
23. Wahba, L., Costantino, L., Tan, F.J., Zimmer, A. & Koshland, D. S1-DRIP-seq identifies high expression and polyA tracts as major contributors to R-loop formation. *Genes Dev* **30**, 1327–38 (2016).

24. Briggs, E., Hamilton, G., Crouch, K., Lapsley, C. & McCulloch, R. Genome-wide mapping reveals conserved and diverged R-loop activities in the unusual genetic landscape of the African trypanosome genome. *Nucleic Acids Res* **46**, 11789–11805 (2018).
25. Silva, S., Camino, L.P. & Aguilera, A. Human mitochondrial degradosome prevents harmful mitochondrial R loops and mitochondrial genome instability. *Proc Natl Acad Sci U S A* **115**, 11024–11029 (2018).
26. Bayona-Feliu, A., Casas-Lamesa, A., Reina, O., Bernues, J. & Azorin, F. Linker histone H1 prevents R-loop accumulation and genome instability in heterochromatin. *Nat Commun* **8**, 283 (2017).
27. Xu, W. *et al.* The R-loop is a common chromatin feature of the Arabidopsis genome. *Nat Plants* **3**, 704–714 (2017).
28. Heintz, C. *et al.* Splicing factor 1 modulates dietary restriction and TORC1 pathway longevity in C. elegans. *Nature* **541**, 102–106 (2017).
29. Zhang, S. *et al.* Alternative polyadenylation drives genome-to-phenome information detours in the AMPKalpha1 and AMPKalpha2 knockout mice. *Sci Rep* **8**, 6462 (2018).
30. Sanz, L.A. *et al.* Prevalent, Dynamic, and Conserved R-Loop Structures Associate with Specific Epigenomic Signatures in Mammals. *Mol Cell* **63**, 167–78 (2016).
31. Hatchi, E. *et al.* BRCA1 and RNAi factors promote repair mediated by small RNAs and PALB2-RAD52. *Nature* (2021).
32. Lloyd, J.P., Tsai, Z.T., Sowers, R.P., Panchy, N.L. & Shiu, S.H. A Model-Based Approach for Identifying Functional Intergenic Transcribed Regions and Noncoding RNAs. *Mol Biol Evol* **35**, 1422–1436 (2018).
33. Costantino, L. & Koshland, D. Genome-wide Map of R-Loop-Induced Damage Reveals How a Subset of R-Loops Contributes to Genomic Instability. *Mol Cell* **71**, 487–497 e3 (2018).
34. Teloni, F. *et al.* Efficient Pre-mRNA Cleavage Prevents Replication-Stress-Associated Genome Instability. *Mol Cell* **73**, 670–683 e12 (2019).
35. Litwin, I. *et al.* Error-free DNA damage tolerance pathway is facilitated by the Irc5 translocase through cohesin. *EMBO J* **37**(2018).
36. Feretzaki, M. *et al.* RAD51-dependent recruitment of TERRA lncRNA to telomeres through R-loops. *Nature* **587**, 303–308 (2020).
37. Daza-Martin, M. *et al.* Isomerization of BRCA1-BARD1 promotes replication fork protection. *Nature* **571**, 521–527 (2019).
38. Koury, E., Harrell, K. & Smolikove, S. Differential RPA-1 and RAD-51 recruitment in vivo throughout the C. elegans germline, as revealed by laser microirradiation. *Nucleic Acids Res* **46**, 748–764 (2018).
39. Leon-Ortiz, A.M. *et al.* A Distinct Class of Genome Rearrangements Driven by Heterologous Recombination. *Mol Cell* **69**, 292–305 e6 (2018).
40. Stork, C.T. *et al.* Co-transcriptional R-loops are the main cause of estrogen-induced DNA damage. *Elife* **5**(2016).

41. Hamperl, S., Bocek, M.J., Saldivar, J.C., Swigut, T. & Cimprich, K.A. Transcription-Replication Conflict Orientation Modulates R-Loop Levels and Activates Distinct DNA Damage Responses. *Cell* **170**, 774–786 e19 (2017).
42. Gurumurthy, S. *et al.* The Lkb1 metabolic sensor maintains haematopoietic stem cell survival. *Nature* **468**, 659 – 63 (2010).
43. Gan, B. *et al.* Lkb1 regulates quiescence and metabolic homeostasis of haematopoietic stem cells. *Nature* **468**, 701–4 (2010).
44. Horsley, V., Aliprantis, A.O., Polak, L., Glimcher, L.H. & Fuchs, E. NFATc1 balances quiescence and proliferation of skin stem cells. *Cell* **132**, 299–310 (2008).
45. Hong, Y., Roy, R. & Ambros, V. Developmental regulation of a cyclin-dependent kinase inhibitor controls postembryonic cell cycle progression in Caenorhabditis elegans. *Development* **125**, 3585–97 (1998).
46. Kadekar, P. & Roy, R. AMPK regulates germline stem cell quiescence and integrity through an endogenous small RNA pathway. *PLoS Biol* **17**, e3000309 (2019).
47. Shilatifard, A. The COMPASS family of histone H3K4 methylases: mechanisms of regulation in development and disease pathogenesis. *Annu Rev Biochem* **81**, 65–95 (2012).
48. Butuci, M., Williams, A.B., Wong, M.M., Kramer, B. & Michael, W.M. Zygotic Genome Activation Triggers Chromosome Damage and Checkpoint Signaling in C. elegans Primordial Germ Cells. *Dev Cell* **34**, 85–95 (2015).
49. Wong, M.M., Belew, M.D., Kwieraga, A., Nhan, J.D. & Michael, W.M. Programmed DNA Breaks Activate the Germline Genome in Caenorhabditis elegans. *Dev Cell* **46**, 302–315 e5 (2018).
50. Blythe, S.A. & Wieschaus, E.F. Zygotic genome activation triggers the DNA replication checkpoint at the midblastula transition. *Cell* **160**, 1169–81 (2015).
51. Roberts, S.A. & Gordenin, D.A. Hypermutation in human cancer genomes: footprints and mechanisms. *Nat Rev Cancer* **14**, 786–800 (2014).
52. Matic, I., Rayssiguier, C. & Radman, M. Interspecies gene exchange in bacteria: the role of SOS and mismatch repair systems in evolution of species. *Cell* **80**, 507–15 (1995).
53. Zahradka, K. *et al.* Reassembly of shattered chromosomes in Deinococcus radiodurans. *Nature* **443**, 569 – 73 (2006).
54. Garcia-Pichardo, D. *et al.* Histone Mutants Separate R Loop Formation from Genome Instability Induction. *Mol Cell* **66**, 597–609 e5 (2017).
55. Bolger, A.M., Lohse, M. & Usadel, B. Trimmomatic: a flexible trimmer for Illumina sequence data. *Bioinformatics* **30**, 2114–20 (2014).
56. Li, H. & Durbin, R. Fast and accurate long-read alignment with Burrows-Wheeler transform. *Bioinformatics* **26**, 589 – 95 (2010).
57. Li, H. *et al.* The Sequence Alignment/Map format and SAMtools. *Bioinformatics* **25**, 2078–9 (2009).

58. Heinz, S. *et al.* Simple combinations of lineage-determining transcription factors prime cis-regulatory elements required for macrophage and B cell identities. *Mol Cell* **38**, 576–89 (2010).
59. Zhang, Y. *et al.* Model-based analysis of ChIP-Seq (MACS). *Genome Biol* **9**, R137 (2008).
60. Sun, B., Fan, P., Liao, M. & Zhang, Y. Modeling endophilin-mediated Abeta disposal in glioma cells. *Biochim Biophys Acta Mol Cell Res* **1865**, 1385–1396 (2018).
61. Lerdrup, M., Johansen, J.V., Agrawal-Singh, S. & Hansen, K. An interactive environment for agile analysis and visualization of ChIP-sequencing data. *Nat Struct Mol Biol* **23**, 349–57 (2016).
62. Craig, A.L., Moser, S.C., Bailly, A.P. & Gartner, A. Methods for studying the DNA damage response in the Caenorhabdatis elegans germ line. *Methods Cell Biol* **107**, 321–52 (2012).
63. Salas-Armenteros, I. *et al.* Human THO-Sin3A interaction reveals new mechanisms to prevent R-loops that cause genome instability. *EMBO J* **36**, 3532–3547 (2017).
64. Girard, C., Roelens, B., Zawadzki, K.A. & Villeneuve, A.M. Interdependent and separable functions of Caenorhabditis elegans MRN-C complex members couple formation and repair of meiotic DSBs. *Proc Natl Acad Sci U S A* **115**, E4443-E4452 (2018).
65. Kelly, W.G. & Fire, A. Chromatin silencing and the maintenance of a functional germline in Caenorhabditis elegans. *Development* **125**, 2451–6 (1998).

Figures

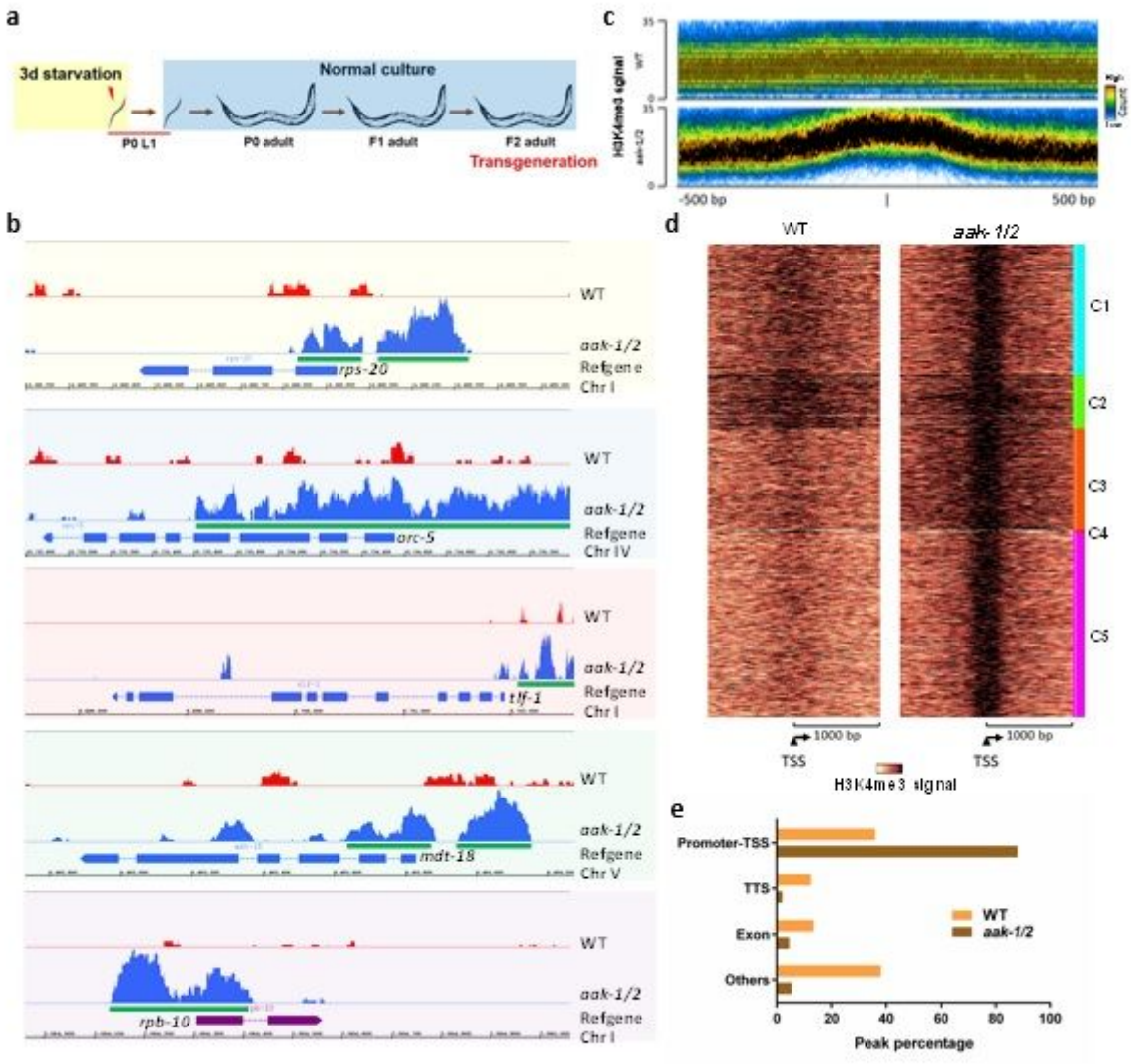

Figure 1

Aberrant H3K4me3 deposition at TSS regions in starved AMPK mutant descendants. a, Sample collection scheme for H3K4me3 ChIP-seq analysis. P0 L1 diapause animals were starved for 3 days in M9 buffer, after which larvae were fed until F2 adult collection. b, Genome browser snapshots of H3K4me3 ChIP-seq signals at the promoter-TSS regions of rps-20, orc-5, tlf-1, mdt-18 and rpb-10 genes. Green bars show promoter-TSS H3K4me3 calls. Track height represents read counts. c, Line tracks of H3K4me3 signal at TSSs. d, k-means clustered heat maps of H3K4me3 signal for WT and aak-1/2 animals at TSS. 5 different clusters were identified at the 1-kb regions flanking the TSS, and densities correspond to H3K4me3 signal. C1-C5, Cluster 1-5. e, Annotation and peak location analyses for called H3K4me peaks mapping to promoter-TSS, TTS, exon, and the other regions. Peak percentage is shown. In aak-1/2 mutants, peaks accumulate at the promoter-TSS fraction, while they decrease dramatically at other regions.

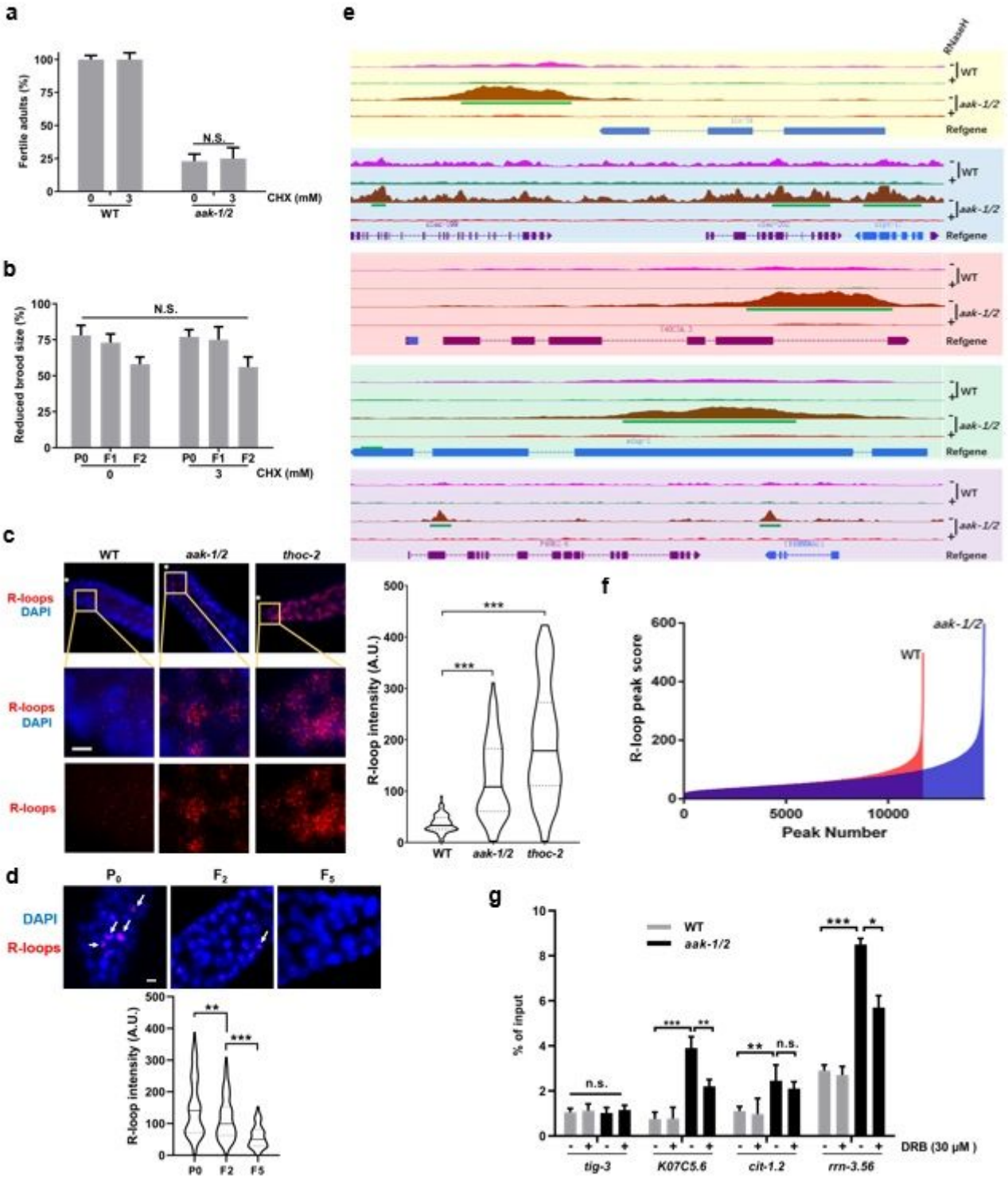

Figure 2

R-loops accumulate within the germ line of starved AMPK mutants. a-b, The observed reproductive phenotypes in post-L1 diapause AMPK mutants are not caused by untimely protein synthesis. a, Emergent WT and aak-1/2 larvae were maintained in M9 buffer containing cyclohexamide (CHX) of indicated concentrations for 3 days before being transferred to replete plates. The proportion of fertile adult animals is represented, n ≥ 150. Error bars represent the confidence interval at 95% (95% CI); N.S.

by Fisher’s exact test. b, Transgenerational brood size defects are not restored in the progeny of post-L1 diapause AMPK mutant larvae treated with CHX during the period of starvation. The frequency of animals with reduced brood size in aak-1/2 mutants and in the subsequent generation (F1 and F2) is represented n ≥ 50. Error bars: 95% CI; N.S. by Fisher’s exact test. c, Left: Schematic drawing of R-loop structure followed by representative micrographs showing R-loops in young adult germ lines of the F2 descendants of starved aak-1/2 mutants (F2) and WT. thoc-2 mutant germ line is shown as a positive control for R-loop detection23. Emergent WT and aak-1/2 L1 larvae were starved 3 days then transferred to replete conditions. Germ lines were fixed and immunostained with S9.6 antibody (red) and counterstained with DAPI (blue). Boxes mark sections that are shown in higher magnification below. (N = 3, n = 100). Asterisk (*) indicates the distal tip cell. Scale bar, 5 μm. Right: Quantification of nuclear RNA-DNA hybrids in the immunofluorescence demonstrated a clear increase in overall R-loop abundance in the germ lines of the F2 descendants of starved aak-1/2 mutants. n = 100. ***p < 0.001 by one-way ANOVA. Mean ± S.E.M. d, R-loops are progressively resolved with successive generations. DNA-RNA hybrids in the nuclei of P0 (n = 83), F2 (n = 100) and F5 (n = 81) germ lines determined by immunofluorescence using the S9.6 antibody. Representative images are shown. Scale bars, 5 N = 2; **p < 0.01, ***p < 0.001 by Mann-Whitney test. (n = 83), F2 (n = 100) and F5 (n = 81) were analyzed by immunofluorescence using the S9.6 antibody. Representative images are shown. Scale bars, 5 μm. N = 2; ∗∗p < 0.01, ∗∗∗p < 0.001 by Mann-Whitney test. e, Genome browser snapshots of DRIP-seq signals at regions proximal to genes and RNaseH tracks. Green bars show R-loop peak calls. Track height represents read counts. f, Overall comparison of DRIP-seq output (peak score and number) in WT versus aak-1/2 genome. g, DRIP-qPCR validation. WT or F2 descendants of starved aak-1/2 mutants with or without DRB treatment during starvation for 3 days were collected for DRIP. tig-3 was selected as negative control. n = 3. Mean ± S.E.M.. Signal values normalized with respect to input genomic DNA are plotted. *p < 0.05, **p < 0.01 by Mann-Whitney U-test.

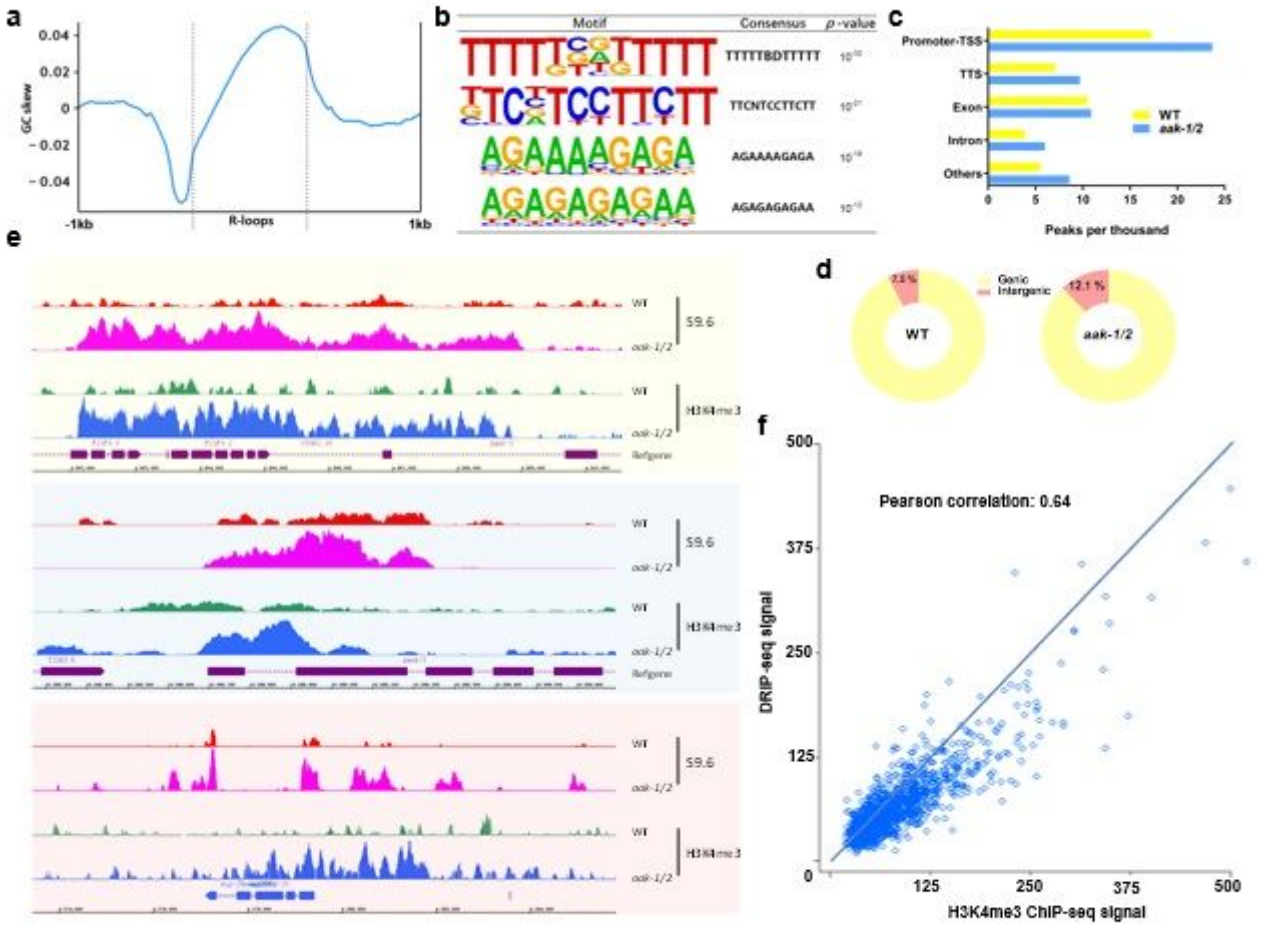

Figure 3

R-loop formation correlates with ectopic deposition of H3K4me3 sites a, Metaplot of GC skew centered on all R-loop peaks. b, Four enriched de novo motifs identified by HOMER analysis of AMPK mutant versus WT DRIP-seq. c, Annotation and peak location analyses for called R-loop peaks mapping to promoter-TSS, TTS, exon, intron and the other regions. Genomic peak proportion in per thousand is shown. Peaks accumulate predominantly at the promoter-TSS fraction in the F2 descendants of starved aak-1/2 mutants. d, Pie charts of DRIP-seq signal distribution for genic versus intergenic regions in WT or F2 descendants of starved aak-1/2 mutants. e, Genome browser snapshots showing positively correlated R-loop signals and H3K4me3 levels in the F2 descendants of starved AMPK mutants. f, DRIP-seq and H3K4me3 signals were compared and Pearson correlation coefficients were calculated using Reads Per Kilobase Million (RPKM) values for 1-kb-binned regions of the whole genome.

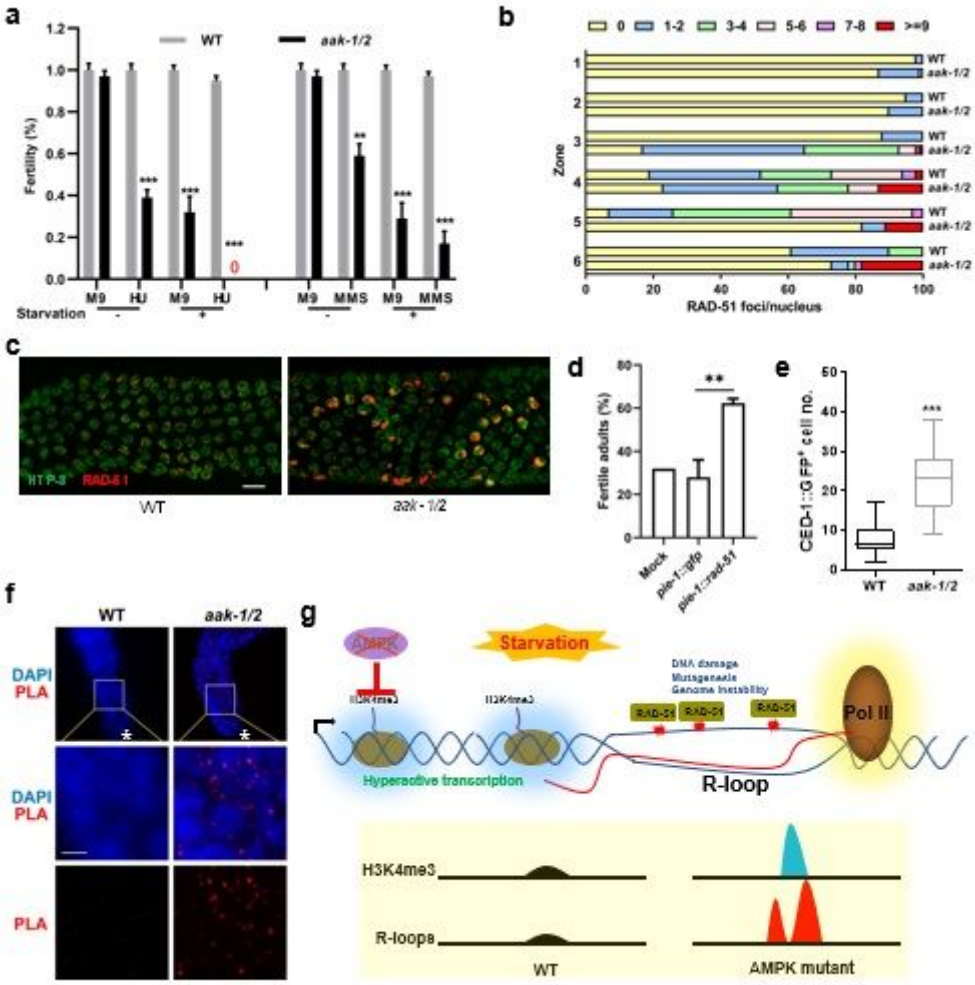

Figure 4

R-loops sequester RAD-51 to compromise fertility and germ cell integrity in starved AMPK mutants a, AMPK mutant L1 larvae are sensitive to genotoxic stress and become hypersensitive following starvation. L1 larvae that were starved or fed for 4 hours were subjected to 25 mM hydroxyurea (HU) and 0.01% methyl methanesulfonate (MMS) at sub-threshold concentrations previously determined to cause sterility in wild-type animals 35. Mean ± S.E.M.. ***p < 0.001, **p < 0.01, *p < 0.05 by unpaired t-test with Welch's correction. Significant differences are shown for comparison between wild type and mutant animals, and with or without starvation. Each assay was independently performed at least thrice. b, Quantification of number and time of appearance of RAD-51 foci in six zones of the germ line: mitotic, transition zone, early pachytene, mid-pachytene, late pachytene and diplotene. WT, n=5. aak-1/2, n=12. c, Representative micrographs showing RAD-51 foci in the pachytene of young adult germ lines of F2 descendants of starved aak-1/2 mutants (F2) and WT. Emergent WT and aak-1/2 L1 larvae were starved 3 days then transferred to replete conditions. Germ lines were fixed and immunostained with RAD-51 antibody (green) and counterstained with DAPI (blue). Images show the RAD-51 foci in the late pachytene regions. Note the distinctive abnormal disorganized morphology of the previously starved aak-1/2 mutant gonads. Scale bar, 5 µm. d, multicopy arrays of rad-51 can partially restore post-starvation fertility in AMPK

mutants. Germline expression of rad-51 was driven by a pie-1 promoter assembled into complex arrays65. Transgenic animals were starved in M9 buffer for 72 hr at 20°C. Animals were then recovered to replete conditions. The percent fertility was assessed 96 hr following recovery. Error bars represent the SD. **p < 0.001 when compared to controls using unpaired t-test. n = 25. e, Cell death is increased in the gonads of the F2 descendants of starved WT versus AMPK mutants. Apoptotic bodies were quantified by counting CED-1::GFP positive cells in the gonad arms (Supplementary Fig. 8c). Box plots show median, boxes 50% and whiskers 90% of the group. n = 50. ***p < 0.001 by Student's t-test. f, Abnormally abundant RAD-51 signals overlap with R-loops in the germ cells of previously starved AMPK mutants. Proximity Ligation Assay (PLA) was used to determine regions where both R-loops and RAD-51 signals overlap indicating potential sites of damage/repair in the adult germ lines of F2 descendants of starved WT versus AMPK mutants. PLA signals are indicated by red spots. Asterisk (*) indicates the distal tip cell. Scale bar, 5 μm. g, Model depicting AMPK-dependent events that occur during acute starvation. AMPK constrains inappropriate H3K4me3 deposition and consequent transcription that causes increases R-loop formation and genomic instability.

Supplementary Files

This is a list of supplementary files associated with this preprint. Click to download.

- SupplementaryFig.1.pptx
- SupplementaryFig.2.pptx
- SupplementaryFig.3.pptx
- SupplementaryFig.4.pptx
- SupplementaryFig.5.pptx
- SupplementaryFig.6.pptx
- SupplementaryFig.7.pptx
- SupplementaryFig.8.pptx